# Role of the target orientation angle and orbital angular momentum in the evaporation residue production

Giovanni FAZIO, Giorgio GIARDINA *, Francis HANAPPE[1], Giuseppe MANDAGLIO, Marina MANGANARO, Akhtam I. MUMINOV[2], Avazbek K. NASIROV[2,3], and Carmelo SACCÁ[4]

*INFN, Sezione di Catania, and Dipartimento di Fisica dell'Università di Messina, Messina, Italy*

[1] *Université Libre de Bruxelles, Bruxelles, Belgium*

[2] *Department of Heavy Ion Physics, Institute of Nuclear Physics, Tashkent, Uzbekistan*

[3] *Joint Institute for Nuclear Research, Dubna, Russia*

[4] *Dipartimento di Scienze della Terra dell'Università di Messina, Messina, Italy*

The influence of the orientation angles of the target nucleus symmetry axis relative to the beam direction on the production of the evaporation residues is investigated for the $^{48}$Ca+$^{154}$Sm reaction as a function of the beam energy. At low energies ($E_{\rm c.m.}$ <137 MeV), the yield of evaporation residues is observed only for collisions with small orientation angles ($\alpha_T < 45^0$). At large energies (about $E_{\rm c.m.}$ =140–180 MeV) all the orientation angles $\alpha_T$ can contribute to the evaporation residue cross section $\sigma_{ER}$ in the 10–100 mb range, and at $E_{c.m.}$ >180 MeV $\sigma_{ER}$ ranges around 0.1–10 mb because the fission barrier for a compound nucleus decreases by increasing its excitation energy and angular momentum.

KEYWORDS: Fusion, quasifission, evaporation residues, orientation of reactants

## 1. Introduction

The study of the role of the entrance channel dynamics in the formation of the evaporation residues (ER) in reactions with massive nuclei is an actual problem in establishing the conditions to obtain new superheavy elements or new isotopes far from the island of stability of chemical elements. The main requirements to reach maximal cross sections in the formation of the evaporation residues are as small as possible values of the excitation energy and angular momentum of the being formed compound nucleus with large fusion probability. In the cold fusion reactions the main requirements have been satisfied and 1n- and 2n-reactions (by emission of one or two neutrons from the compound nucleus) leaded to observe events confirming the synthesis of superheavy elements $Z$=110 (darmstadtium), 111 (roentgenium) and 112 (see Refs.[1,2]), as well as element $Z$=113 (see Ref.[3]). The events proving the synthesis of heavier new elements $Z$=114, 115, 116, 118 were observed in the hot fusion reactions with $^{48}$Ca on the actinide targets $^{244}$Pu, $^{243}$Am, $^{248}$Cm and $^{249}$Cf, respectively, in which the excitation energy of the compound nucleus was more than 35 MeV.[4] There is an opinion that

*E-mail address: giardina@nucleo.unime.it

the values of beam energy leading to the observed maximal cross sections correspond to the equatorial collisions of the deformed actinide targets[5] (the orientation angle of the nucleus symmetry axis to the beam direction is 90°). The results of our calculations showed that the maximal cross sections should be observed at orientation angles less than 90° because of influence of the entrance channel on the dynamics of capture.[6] Therefore, to investigate the evaporation residue production, it is important to analyze the role of the entrance channel characteristics such as the beam energy, orbital angular momentum, orientation angles of the symmetry axes of the projectile and target nuclei relative to the beam direction in the angular momentum distribution of the excited compound nucleus. Although the reaction cross section for the interaction of massive nuclei is enough large, only very small part ($\sigma_{ER}/\sigma_{react} \sim 10^{-9}$) can belong to the expected ER events at synthesis of superheavy elements $Z > 108$.[1,4] In fact, the complete fusion of two massive nuclei is in competition with the quasifission (QF) process[7] (re-separation of the interacting system into two fragments without reaching compound nucleus) during the first stage of the reaction, while the evaporation process (leading to the evaporation residue nuclei) competes with the fission process along the de-excitation cascade of the compound nucleus (CN). Moreover, at the large values of angular momentum ($\ell > 82$), also the fast-fission (FF) can contribute to the formation of nuclear fragments hindering the ER formation.

In this paper we present the results of our study on the $^{48}$Ca+$^{154}$Sm reaction showing as the orientation angle of the symmetry axis of the target nucleus relative to the beam direction and orbital angular momentum affect the yields of the evaporation residues.

## 2. Method

We use the method developed in our previous papers[8–11] to describe the role of the all three stages starting from the dinuclear system (DNS) formation at capture of the projectile by the target-nucleus, then its evolution into a compound nucleus and the production of the evaporation residues after emission of gamma-quanta, neutrons, protons, $\alpha$-particles. The method allows us to determine the corresponding cross sections of capture, complete fusion and formation of the evaporation residues. By this method we are able to determine the angular momentum distribution of the DNS (determined by the conditions of the entrance channel) and competition between quasifission and complete fusion affected by the conditions of the reaction mechanism. Therefore, also the de-excitation chain of the compound nucleus (characterized by the fission-evaporation competition) is affected by the reaction dynamics.[12,13]

### *2.1 Collision of spherical nuclei*

It is worth to calculate the cross section of evaporation residues which can be compared with the corresponding experimental data. The probability of formation of the evaporation residue nucleus being survived with mass number $A = A_{CN} - (\nu(x) + y(x) + 4k(x))$ and charge number $Z = Z_{CN} - (y(x) + 2k(x))$ from the heated and rotated compound nucleus $^{A_{CN}}Z_{CN}$

after emissions of $\nu$ neutrons, $y$ protons, $k$ $\alpha$-particles at the $x$th step of the de-excitation cascade by the formula:[12,14]

$$\sigma_{ER(x)}(E^*_x) = \sum_{\ell=0}^{\ell_f}(2\ell+1)\sigma^{\ell}_{(x-1)}(E^*_x)W_{\mathrm{sur}(x-1)}(E^*_x,\ell), \tag{1}$$

where $\sigma^{\ell}_{(x-1)}(E^*_x)$ is the partial cross section of the intermediate nucleus formation at the $(x-1)$th step and $W_{\mathrm{sur}(x-1)}(E^*_x,\ell)$ is the survival probability of the $(x-1)$th intermediate nucleus against fission along the de-excitation cascade of CN; $\ell_f$ is the value of angular momentum $\ell$ at which the fission barrier for a compound nucleus disappears completely;[15] $E^*_x$ is an excitation energy of the nucleus formed at the $x$th step of the de-excitation cascade. It is clear that $\sigma^{\ell}_{(0)}(E^*_0) = \sigma^{\ell}_{\mathrm{fus}}(E^*_{CN})$ at

$$E^*_{CN} = E^*_0 = E_{\mathrm{c.m.}} + Q_{gg} - E_{rot}, \tag{2}$$

where $E_{\mathrm{c.m.}}$, $Q_{gg}$, and $E_{rot}$ are the collision energy in the center of mass system, the reaction $Q_{gg}$-value and rotational energy of the compound nucleus, respectively. The numbers of the being emitted neutrons, protons, $\alpha$-particles and $\gamma$-quanta, $\nu(x)$n, $y(x)$p, $k(x)\alpha$, and $s(x)\gamma$, respectively, are functions of the step $x$. The emission branching ratios of these particles depend on the excitation energy $E^*_A$ and angular momentum $\ell_A$ of the being cooled intermediate nucleus.

The chain of the de-excitation cascade, characterized by the emission of the above-mentioned particles, starts from the compound nucleus ${}^{A_{CN}}Z_{CN}$. Its formation probability is the partial cross section of complete fusion $\sigma^{\ell}_{\mathrm{fus}}(E^*_{CN})$ corresponding to the orbital angular momentum $\ell$. The fusion cross section is equal to the capture cross section for the light systems or light projectile induced reactions while for the reactions with massive nuclei it becomes a model dependent quantity. Concerning the estimation of the fusion cross section from the experimental data of fragments, sometimes, its value is an ambiguous quantity because of difficulties in separation of the fusion-fission fragments from the quasifission fragments in the case of overlap of their mass and angular distributions.

In our model, we calculate $\sigma^{\ell}_{\mathrm{fus}}(E^*_{CN})$ by estimation of the competition of the complete fusion with quasifission if we know the partial capture cross section:

$$\sigma^{\ell}_{\mathrm{fus}}(E_{\mathrm{c.m.}}) = \sigma^{\ell}_{cap}(E_{\mathrm{c.m.}})P_{\mathrm{CN}}(E_{\mathrm{c.m.}},\ell), \tag{3}$$

where $P_{CN}(E_{\mathrm{c.m.}})$ is the hindrance factor for the formation of the compound nucleus connected with the competition between complete fusion and quasifission as possible channels of evolution of the DNS. Note $E_{\mathrm{c.m.}}$ and $E^*_{CN}$ are connected by relation (2). Details of the calculation method are described in ref.[14]

The partial capture cross section at given energy $E_{\mathrm{c.m.}}$ and orbital angular momentum $\ell$ is determined by the formula:

$$\sigma^{\ell}_{cap}(E_{\mathrm{c.m.}}) = \pi\lambda\!\!\!^{-2}\mathcal{P}^{\ell}_{cap}(E_{\mathrm{c.m.}}) \tag{4}$$

where $\mathcal{P}^{\ell}_{cap}(E_{\rm c.m.})$ is the capture probability for the colliding nuclei to be trapped into the well of the nucleus-nucleus potential after dissipation of a part of the initial relative kinetic energy and orbital angular momentum. The capture probability $\mathcal{P}^{\ell}_{cap}$ is equal to 1 or 0 for given $E_{\rm c.m.}$ energy and orbital angular momentum $\ell$. Our calculations showed that in dependence on the center-of-mass system energy $E_{\rm c.m.}$ there is a "window" of the orbital angular momentum for capture with respect to the following conditions:[6,16]

$$\mathcal{P}^{\ell}_{cap}(E_{\rm c.m.}) = \begin{cases} 1, \ \text{if} \ \ \ell_{\rm min} \le \ell \le \ell_{\rm d} \ \ \text{and} \ \ E_{\rm c.m.} > V_{\rm Coul} \\ 0, \ \text{if} \ \ \ell < \ell_{\rm min} \ \ \text{or} \ \ \ell > \ell_{\rm d} \ \text{and} \ \ E_{\rm c.m.} > V_{\rm Coul} \\ 0, \ \text{for all} \ \ell \quad \text{if} \ \ E_{\rm c.m.} \le V_{\rm Coul} \, . \end{cases}$$

The boundary values $\ell_{min}$ and $\ell_d$ of the partial waves leading to capture depend on the dynamics of collision and they are determined by solving the equations of motion for the relative distance $R$ and orbital angular momentum $\ell$.[8,10,11] At lower energies $\ell_{min}$ goes down to zero and we don't observe the $\ell$ "window": $0 \le \ell \le \ell_d$. The range of the $\ell$ "window" is defined by the size of the potential well of the nucleus-nucleus potential $V(R, Z_1, Z_2)$ and the values of the radial $\gamma_R$ and tangential $\gamma_t$ friction coefficients, as well as by the moment of inertia for the relative motion.[6,8] The capture cross section is determined by the number of partial waves that lead colliding nuclei to trap into the well of the nucleus-nucleus potential after dissipation of the sufficient part of the initial kinetic energy (see for example Fig. 1(a) of Ref.[16]). The size of the potential well decreases by increasing the orbital angular momentum, $\ell$. The value of $\ell$ at which the potential well disappears is defined as the critical value $\ell_{cr}$. In some models, it is assumed as the maximum value of the partial waves giving contribution to the complete fusion. But, unfortunately, this is not true: the use of $\ell_{cr}$, as a maximum value of $\ell$ contributing to capture, leads to the overestimation of the capture and fusion cross sections. Because at $\ell_d < \ell \le \ell_{cr}$ the deep inelastic collisions take place (see Fig. 1(b) of Ref.[16]). It should be stressed that such a process occurs because of the limited values of the radial friction coefficient,[8,9,17] the capture becomes impossible at the low values of the orbital angular momentum if the beam energy values are enough high than the Coulomb barrier.

### *2.2 Collision of deformed nuclei*

Due to the dependence of the nucleus-nucleus potential ($V$) and moment of inertia ($J_R$) for DNS on the orientations of the symmetry axes of deformed nuclei, the excitation functions of the capture and fusion are sensitive to the orientations under discussion. This was demonstrated in Ref.[6] The present paper is devoted to the study of the dependence of the evaporation residue cross section on the orientation angles of the deformed interacting nuclei. Certainly, it is impossible directly to establish the above-mentioned dependence by an experimental way. But the theoretical analysis allows us to estimate the contributions of collisions by different orientation angles to the measured evaporation residue cross sections. Conclusions of such kind of analysis are useful to find favourable beam energies for the synthesis of

superheavy elements in reactions with deformed nuclei.

Usually, the final results of the evaporation residue cross sections are obtained by averaging the contributions calculated for the different orientation angles of the symmetry axes of the deformed reacting nuclei (as used in Ref.[18])

$$< \sigma_{ER}(E_{\rm c.m.}) >= \int_0^{\pi/2} \sin\alpha_P \int_0^{\pi/2} \sigma_{ER}(E_{\rm c.m.};\alpha_P,\alpha_T)) \sin\alpha_T d\alpha_P d\alpha_T \tag{5}$$

where $\sigma_{ER}(E_{\rm c.m.};\alpha_P,\alpha_T)$ is calculated by the formula (1) for the all considered orientation angles of the symmetry axes of the projectile and target nuclei.

*2.3 Including surface vibration of spherical nucleus*

The projectile used in the reaction under consideration is the double magic spherical nucleus $^{48}$Ca. But our results did not describe experimental data at low energies if we use spherical shape for $^{48}$Ca. Therefore, we take into account the fluctuation of its shape around the spherical shape due to the zero-point motion connecting by the quadrupole and octupole excitations. We calculated capture and fusion cross sections with different vibrational states of $^{48}$Ca $\beta_\lambda = -\beta_\lambda^{(0)}, -\beta_\lambda^{(0)} + \Delta\beta, ..., \beta_\lambda^{(0)}$, where $\lambda = 2, 3$. Then we performed averaging of the capture and fusion cross sections over the values of the shape parameters used in calculations:

$$< \sigma_i(E_{\rm c.m.},\alpha_T) >= \int_{-\beta_2^{(0)}}^{\beta_2^{(0)}} \int_{-\beta_3^{(0)}}^{\beta_3^{(0)}} \sigma_i(E_{\rm c.m.};\beta_2^{(P)},\beta_3^{(P)},\alpha_T) g(\beta_2^{(P)},\beta_3^{(P)}) d\beta_2^{(P)} d\beta_3^{(P)}, \tag{6}$$

with $i = cap,\ fus$ and with the weight function[19]

$$g(\beta_2^{(P)},\beta_3^{(P)}) = \exp\left[-\frac{(\sum_\lambda \beta_\lambda^{(P)} Y_{\lambda 0}^*(\alpha_P))^2}{2{\sigma_{\beta_P}}^2}\right] \left(2\pi\sigma_{\beta_P}^2\right)^{-1/2} \tag{7}$$

where $\beta_\lambda^{(P)}$ is a current value of the deformation parameters characterizing the shape of the nucleus; for simplicity hereafter we use $\beta_P = \{\beta_2^{(P)}, \beta_3^{(P)}\}$ characterizing the parameters of the first collective vibrational states $2^+$ and $3^-$, respectively; $\alpha_P$ is the direction of the symmetry axis of the projectile shape when it has prolate ($\beta_2^{(P)} > 0$) or oblate ($\beta_2^{(P)} < 0$) deformation. It is assumed $\alpha_P = 0$ in our calculations. The dispersion of the shape fluctuations is calculated by the formula

$$\sigma_{\beta_P}^2 = \sum_{n\lambda} \frac{2\lambda+1}{4\pi} \frac{\hbar}{2D_{n\lambda}\omega_{n\lambda}}. \tag{8}$$

for the case $n = 1$ and $\lambda = 2$ in $^{48}$Ca.

The amplitudes $\beta_2^{(0)}$, $\beta_3^{(0)}$, excitation energies of the first vibrational states $2^+$ and $3^-$ are taken from Refs.,[20,21] respectively; $D_\lambda = \hbar/(2\omega_\lambda(\beta_\lambda)^2)$.

The results obtained by (6) were used in the following formula

$$< \sigma_{ER}(E_{\rm c.m.}) >= \int_0^{\pi/2} \sigma_{ER}(E_{\rm c.m.};\alpha_T) \sin\alpha_T d\alpha_T \tag{9}$$

to calculate the evaporation residue cross section by averaging only on the different orientation angles of the symmetry axis $\alpha_T$ of the deformed target nucleus. The fusion excitation function

is determined by product of the partial capture cross section $\sigma_{cap}^{\ell}$ and fusion probability $P_{CN}$ of DNS at various $E_{\rm c.m.}$ values:

$$\sigma_{fus}(E_{\rm c.m.};\beta_P,\alpha_T)=\sum_{\ell=0}^{\ell_f}(2\ell+1)\sigma_{cap}(E_{\rm c.m.},\ell;\beta_P,\alpha_T)P_{CN}(E_{\rm c.m.},\ell;\beta_P,\alpha_T). \quad (10)$$

Obviously, the quasifission cross section is defined by

$$\sigma_{qfis}(E_{\rm c.m.};\beta_P,\alpha_T)=\sum_{\ell=0}^{\ell_d}(2\ell+1)\sigma_{cap}(E_{\rm c.m.},\ell;\beta_P,\alpha_T)(1-P_{CN}(E_{\rm c.m.},\ell;\beta_P,\alpha_T)). \quad (11)$$

Another binary process which leads to the formation of two fragments similar to fragments of fusion-fission or quasifission is the fast-fission. It occurs only at high values of the angular momentum $\ell > \ell_f$ at which the rotating nucleus has not the fission barrier and becomes unstable against fission.[15] It is a disintegration into two fragments of the fast rotating mononucleus which has survived against quasifission (the decay of the DNS into two fragments without formation of the compound nucleus). Therefore, the mononucleus having high values of the angular momentum, splits into two fragments immediately if its angular momentum is larger than $\ell_f$, because there is not a barrier providing stability. The fast-fission cross section is calculated by summing of contributions of the partial waves corresponding to the range $\ell_f \le \ell \le \ell_d$ leading to the formation of the mononucleus:

$$\sigma_{fast-fis}(E_{\rm c.m.};\beta_P,\alpha_T)=\sum_{\ell_f}^{\ell_d}(2\ell+1)\sigma_{cap}(E_{\rm c.m.},\ell;\beta_P,\alpha_T)P_{CN}(E_{\rm c.m.},\ell;\beta_P,\alpha_T). \quad (12)$$

The capture cross section in the framework of the DNS model is equal to the sum of the quasifission, fusion-fission and fast-fission cross sections:

$$\sigma_{cap}^{\ell}(E_{\rm c.m.};\beta_P,\alpha_T)=\sigma_{qfiss}^{\ell}(E_{\rm c.m.};\beta_P,\alpha_T)+\sigma_{fus}^{\ell}(E_{\rm c.m.};\beta_P,\alpha_T)+\sigma_{fast-fis}^{\ell}(E_{\rm c.m.};\beta_P,\alpha_T). \quad (13)$$

It is clear that fusion cross section includes the cross sections of evaporation residues and fusion-fission products. The fission cross section is calculated by the advanced statistical code[14,22,23] that takes into account the damping of the shell correction in the fission barrier as a function of the nuclear temperature and orbital angular momentum.

## 3. Results of the $^{48}$Ca+$^{154}$Sm reaction

In order to investigate the influence of the angular orientations of the interacting nuclei on the evaporation residue yields, we choose the $^{48}$Ca+$^{154}$Sm reaction because the experimental data of the evaporation residue cross sections for this reaction are presented in Ref.[24] Therefore, a good description of the measured ER cross section in the framework of our model taking into account the three stages of the fusion-fission reactions allows us to describe in detail the preceding mechanism leading to the formation of the ER nuclei.

We study the dependence of the competition between quasifission and complete fusion on the orientation angle $\alpha_T$ of the symmetry axis of the target nucleus. The quadrupole deformation parameter of $^{154}$Sm is equal to 0.27 at the ground state. Although $^{48}$Ca is spherical, in our calculations we take into account the first quadrupole ($2^+$) and octupole ($3^-$) collective excitations as fluctuations around the spherical shape with the amplitudes $< \beta_2^{(+)} >= 0.101$ (from Ref.[20]) and $< \beta_3^{(-)} >=0.25$ (from Ref.[21]), respectively.

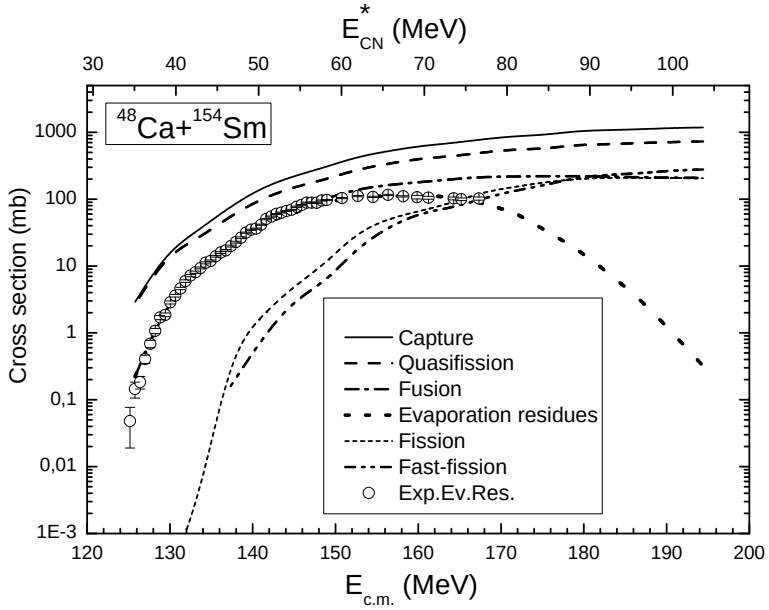


Fig. 1. Theoretical excitation functions for capture (solid line),quasifission (dashed line), fusion (dot-dashed line), evaporation residue (thick short dashed line), fission (thin short-dashed line) and fast-fission (dash-double dotted line) versus the collision energy $E_{\rm c.m.}$ in the center-of-mass system for the $^{48}$Ca+$^{154}$Sm reaction leading to the $^{202}$Pb compound nucleus. Open circles are the experimental data of the evaporation residues taken from Ref.[24]

Fig. 1 shows the capture, quasifission, fusion and evaporation residue cross sections. The complete fusion cross section includes only the angular momentum values $\ell < \ell_f$ (see in forward Fig. 5) because the compound nucleus becomes unstable against fission for $\ell > \ell_f$ (where $\ell_f = 82\hbar$ for $^{202}$Pb) and appears the fast-fission. In this figure we also present the fission and fast-fission cross sections that become appreciable at higher values of $E_{\rm c.m.}$. The theoretical results for the formation of evaporation residues were obtained by using formula (9). The good agreement between our results for ER and the experimental data of Ref.[24] is reached by using the formulae for the effective radii of the proton ($R_p$) and neutron ($R_n$) distributions[25] in the nucleus as a function of the their atomic $A$ and charge $Z$ numbers to calculate the nucleus radius:

$$R_{nucleus}(A,Z) \quad = \quad k\sqrt{(ZR_p^2 + (A-Z)R_n^2)/A}, \tag{14}$$

where

$$R_p(A,Z) = 1.237(1-0.157(A-2Z)/A-0.646/A)A^{1/3}, \quad (15)$$

$$R_n(A,Z) = 1.176(1+0.25(A-2Z)/A+2.806/A)A^{1/3}. \quad (16)$$

In our calculations we used the coefficient $k$=0.917. The capture and fusion cross sections depend on the radius parameter due to the nucleus-nucleus interaction potential $V(R)$ between reactants. $V(R)$ is calculated by the double folding procedure over the nucleon distribution functions of the interacting nuclei with the effective Migdal's nucleon-nucleon forces.[8,26] The nucleon distribution function of the target-nucleus is as follows:[8,11]

$$\rho_T^{(0)}(\mathbf{r};A,Z) = \rho_0\left\{1+\exp\left[\frac{r-\tilde{R}_T(\beta_2,\beta_3;\alpha_T,A,Z)}{a}\right]\right\}^{-1}, \quad (17)$$

$$\tilde{R}_T(\beta_2,\beta_3;A,Z,\alpha_T) = R_T(A,Z)\left(1+\beta_2 Y_{20}(\alpha_T)+\beta_3 Y_{30}(\alpha_T)\right),$$

where $\rho_0$=0.17 fm$^{-3}$ and $a$=0.54 fm. As we stressed above in the subsection 2.1, the capture probability for the given values of $E_{\rm c.m.}$ and $\ell$ is determined by the size of the potential well of $V(R)$. The depth of the latter is used as the quasifission barrier $B_{qf}$ in our calculations of the fusion and quasifission cross sections.[8,10–12] The fusion cross section depends also on the intrinsic fusion barrier $B^*_{fus}$ for the given mass asymmetry of dinuclear system. The definition of $B^*_{fus}$ and its dependence on the orientation angle $\alpha_T$ will be discussed later (see Fig. 9). The values of $B^*_{fus}$ is determined from the landscape of the potential energy surface which includes $V(R)$. This short comment is to explain the role of nuclear radius in calculations of the evaporation residues cross section obtained by the relation (1).

The ER data are comparable with the fusion cross section at $E_{\rm c.m.}$ energies lower than 150 MeV while at the energies $E_{\rm c.m.}$ >165 MeV the fission cross section overcomes the one of the total evaporation residues becoming comparable with the fusion cross section (see Fig. 1). Also the fast-fission cross section becomes appreciable at energies $E_{\rm c.m.}$ >165 MeV while the evaporation residue cross section decreases. Such a decrease of $\sigma_{ER}$ is connected with the fact that the fission barrier for a compound nucleus decreases by increasing its excitation energy $\mathrm{E}^*_{CN}$[10,11] and angular momentum $\ell$.[15] Therefore, the survival probability of the heated and rotating nuclei along the de-excitation cascade of CN strongly decreases.

Before the analysis of the contributions of the different orientation angles $\alpha_T$ of the symmetry axis of the $^{154}$Sm target to the averaged results for the evaporation residues in Fig. 1 we discuss the dependence of the partial capture and fusion cross sections on $\alpha_T$. The presented results of the dependence on the orientation angle $\alpha_T$ in Figs. 2, 3, 5 and 6 are already multiplied on the weight factor $\sin\alpha_T$ used at averaging procedure by (9).

The upper and lower parts of Fig. 2 show the partial capture ($\sigma^\ell_{cap}$) and fusion ($\sigma^\ell_{fus}$) cross sections, respectively, as a function of the energy $E_{c.m.}$ for some typical orientation angles (for example, at $\alpha_T$=15° for a small angle, and $\alpha_T$=90° for a large angle) of the symmetry axis of

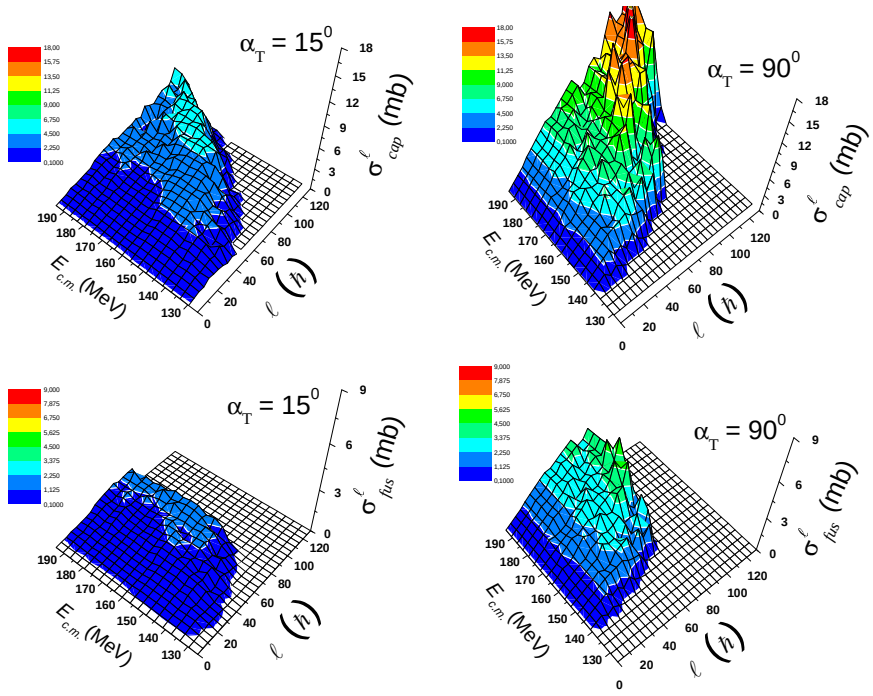


Fig. 2. Spin distribution of the capture (upper part) and fusion (lower part) cross sections as a function of the collision energy $E_{\rm c.m.}$ in the center-of-mass-system and angular momentum $\ell$, at orientation angles $\alpha_T = 15^\circ$ and $90^\circ$. Note that the scale of $\sigma^\ell_{fus}$ is two times smaller than the one for $\sigma^\ell_{cap}$ in order to see in a better way the structure of the $\sigma^\ell_{fus}$ shape.

the deformed $^{154}$Sm target nucleus. The volumes of the distributions strongly depend on the orientation angle $\alpha_T$ of the target.

From Fig. 2 appears that for the considered $^{48}$Ca+$^{154}$Sm reaction the capture yield strongly overcomes the fusion one at each angular configuration $\alpha_T$ because quasifission is the dominant process in the competition with fusion during the evolution of the DNS, due to the relatively small values of the quasifission barrier $B_{qf}$ (see in forward panel (b) of Fig. 8). At low energies (about $E_{c.m.}$ = 125 - 137 MeV) the fusion, reached by the evolution of the DNS, is low and appears for small orientation angles $\alpha_T$ of the target (see low part of Fig. 2, left panel at $\alpha_T = 15^\circ$). Instead, at large values of $\alpha_T$ (see the right panel at $\alpha_T = 90^\circ$) the fusion formation is not possible in the above-mentioned $E_{\rm c.m.}$ energy range. For large orientation angles $\alpha_T$ the fusion process can occur only at larger $E_{\rm c.m.}$ energies due to the large values of the Coulomb barrier (see in forward Fig. 4).

Fig. 3 shows the capture and fusion cross section versus $E_{c.m.}$ for many different orientation angles $\alpha_T$ of the target. This figure shows large capture cross sections at high values of the $E_{c.m.}$ energy. At lower $E_{c.m.}$ energies (at about $E_{c.m.} < 137$ MeV) only the small orientation angles of the target ($\alpha_T \leq 45^\circ$) can give contribute to the capture cross section due to the low values of the Coulomb barrier for the mentioned $\alpha_T$ angle range (see again Fig. 4). At about $E_{c.m.}$=148 MeV all the $\alpha_T$ configurations contribute to the capture cross section approximately with the same possibilities because the collision energy $E_{\rm c.m.}$ is enough to

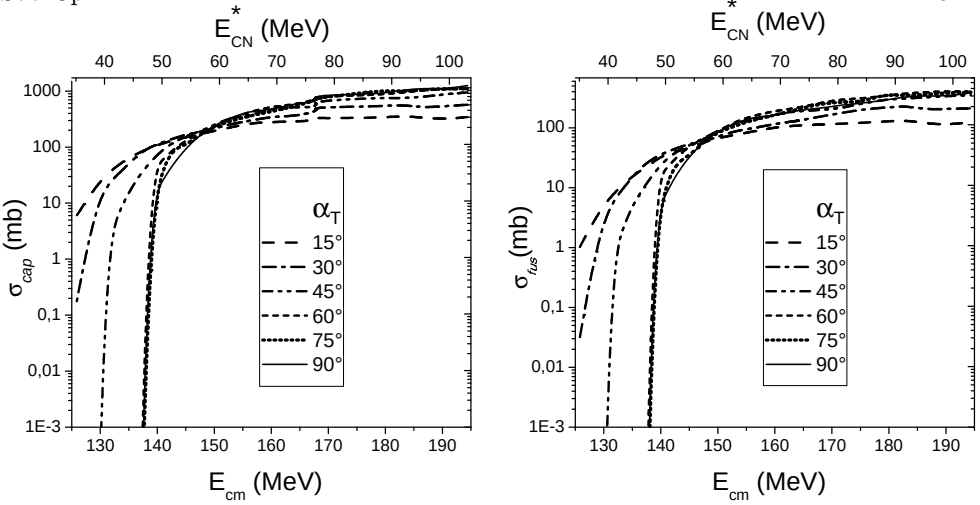


Fig. 3. Capture and fusion cross sections versus the collision energy $E_{\rm c.m.}$ for various target orientation angles $\alpha_T$.

overcome the maximum value of the Coulomb barrier depending by the $\alpha_T$ angle. In the above-mentioned low energy range, also for the fusion cross section can contribute only the small configuration of the target with $\alpha_T \leq 45°$. At higher $E_{\rm c.m.}$ energies (at about $E_{\rm c.m.} >$ 155 MeV) the contributions for the configurations with $\alpha_T \geq 45°$ are larger than the ones with $\alpha_T \leq 30°$ for both the capture and fusion cross sections.

The dependence of the Coulomb barrier on $\alpha_T$ is presented in Fig.4. This phenomenon is evident from the geometry of collision in relation to the relative distance between the centers of the two interacting nuclei. For large orientation angles $\alpha_T$, the capture process can occur

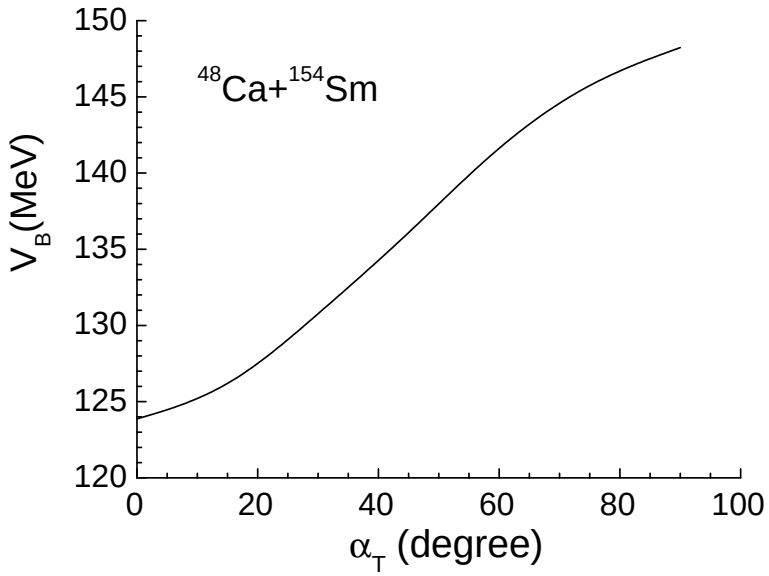


Fig. 4. Coulomb barrier $V$ of the nucleus-nucleus interaction versus the orientation angle $\alpha_T$ of the target nucleus.

at high values of $E_{\rm c.m.}$ only because increases the Coulomb barrier (due to the decrease of

the distance of centers of nuclei by increasing the angle $\alpha_T$) determined by the formula A.2 discussed in Ref.[10] The Coulomb barrier reaches its maximum value $V_B = 148.2$ MeV at $\alpha_T = 90^\circ$ (equatorial collision). Such behaviour of the Coulomb barrier is expected. But a dependence of the hindrance to the complete fusion on $\alpha_T$ is not evident.

In Figs. 5 and 6 are presented the partial cross sections of complete fusion $\sigma^{\ell}_{fus}$ and quasi-fission $\sigma^{\ell}_{qfiss}$, respectively, as a function of the orientation angle $\alpha_T$ for different values of the collision energy in the center-of-mass system. The volumes of the distributions strongly depend on the values of $\alpha_T$. The $\sigma^{\ell}_{qfiss}(E_{\rm c.m.})$ and $\sigma^{\ell}_{fus}(E_{\rm c.m.})$ cross sections are related to the partial capture cross section $\sigma^{\ell}_{cap}(E_{\rm c.m.})$ by the formula (13) which also includes the contribution of the fast-fission cross section $\sigma^{\ell}_{fast-fis}(E_{\rm c.m.})$. From these figures appears that for the considered $^{48}$Ca+$^{154}$Sm reaction the quasifission is the dominate process for all orientation angles $\alpha_T$ of the target-nucleus.

The smallness of the capture and fusion cross sections at small orientation angles $\alpha_T$ is connected with the restriction of the number of partial waves leading to the capture because the entrance channel barrier increases by increasing the DNS rotational energy at given values of $\alpha_T$. This effect is seen from the bottom panels of Figs. 5 and 6. According to the dinuclear system model the depth of the potential well for the given mass asymmetry of reactants is considered as a quasifission barrier $B_{qf}$ keeping DNS from decay into two fragments with the corresponding mass and charge numbers. Peculiarities of such a dependence reflects on the capture cross section and competition between quasifission and complete fusion processes during the evolution of the dinuclear system.

Calculations of dynamics of incoming paths show the following properties of the capture cross section:

– the capture of the projectile by the target nucleus takes place if the collision energy is larger than the Coulomb barrier for each collision with the corresponding orientation angle $\alpha_T$;

– the number of the partial waves which determine the capture cross section increases by increasing the beam energy;

– the number of the partial waves is larger if the depth of the potential well is large;

– the number of the partial waves ceases to increase by increasing the beam energy for the given orientation angle $\alpha_T$ if the beam energy is enough larger than the Coulomb barrier due to the restricted value of the radial friction coefficient. In fact, after dissipation of the relative kinetic energy the projectile could not be trapped into the potential well. So, for small values of the orbital angular momentum and large values of the beam energy we have a "$\ell$-window" because $\ell_{min} > 0$ (see page 4).

We stress that by increasing the beam energy, also increases the possible angular configurations of the deformed target that contribute to the fusion process. At higher energies the

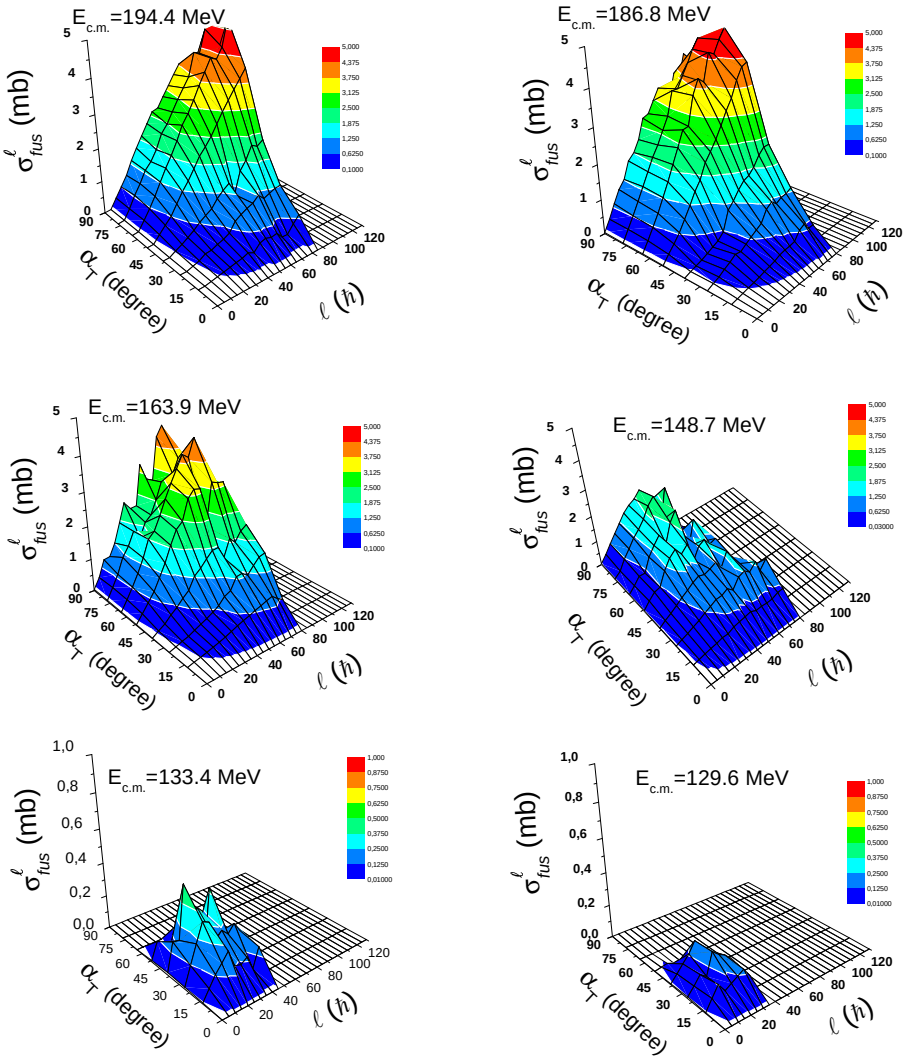


Fig. 5. Partial fusion cross section as a function of the orientation angle $\alpha_T$ of the target nucleus and initial orbital angular momentum $\ell$, at various values of the collision energy $E_{\rm c.m.}$. Note that the scale of the panels at $E_{\rm c.m.}$ = 129.6 and 133.4 MeV is five times smaller than the one of other panels in order to see in a better way the structure of the $\sigma^{\ell}_{fus}$ shape.

rate of the fusion formation at competition between quasifission and fusion increases (see in forward Fig. 7). The reason is connected with the decrease of the intrinsic fusion barrier $B^{*}_{fus}$ by the increase of the orientation angle $\alpha_T$.

The increase of hindrance to the complete fusion at small orientation angles was discussed in Ref.[6] and we observe it clearly for the investigated $^{48}$Ca+$^{154}$Sm reaction. This is connected with the dependence of the potential energy surface, particularly of the driving potential $U_{dr}$, on the orientation angle of the symmetry axis of deformed nucleus relative to the beam direction. As a result the competition between complete fusion and quasifission becomes a function of the angular configuration of the reacting nuclei (see Ref.[6]). For example, the role of the quasifission in reactions with deformed nuclei was discussed in the paper of Hinde *et al.*[27] showing the increase of the anisotropy of the fragment angular distribution at lowest

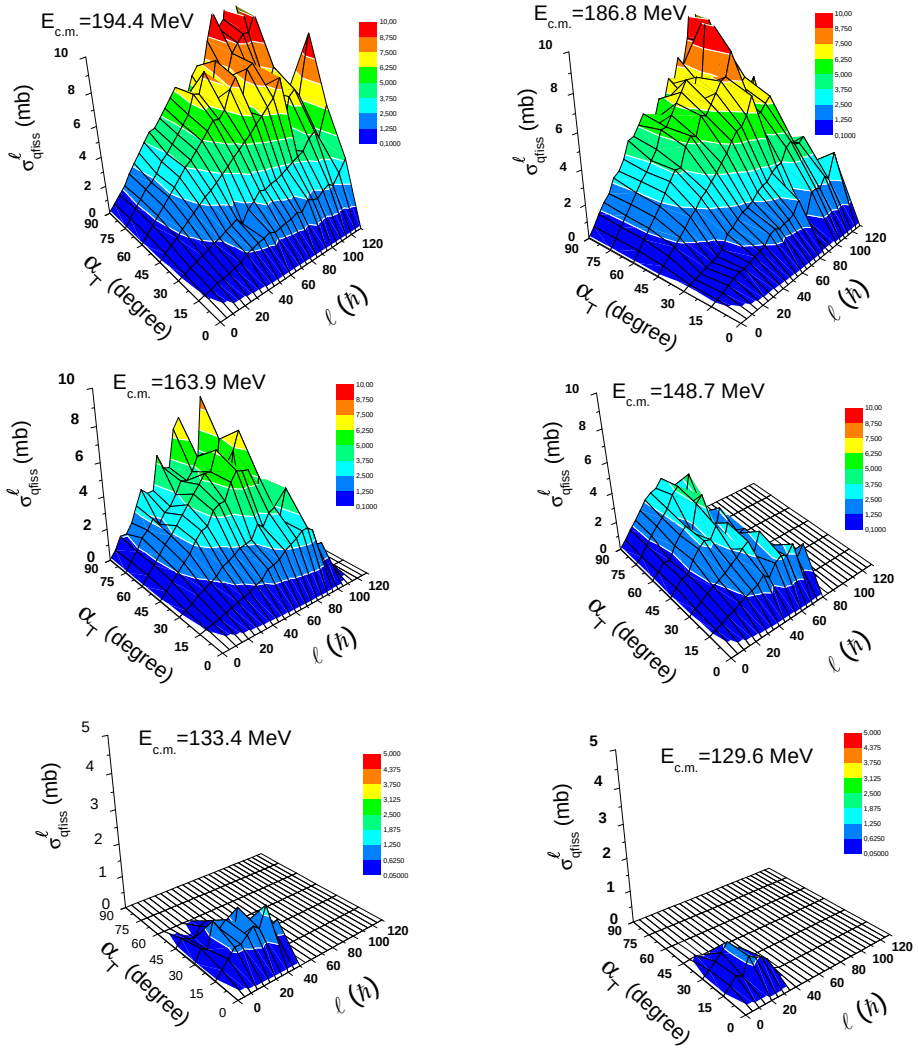


Fig. 6. Partial quasifission cross section as a function of the orientation angle $\alpha_T$ of the target nucleus and initial orbital angular momentum $\ell$, at various values of the collision energy $E_{\rm c.m.}$. Note that the scale of the panels at $E_{\rm c.m.} = 129.6$ and 133.4 MeV is two times smaller than the one of other panels in order to see in a better way the structure of the $\sigma^{\ell}_{qfiss}$ shape.

$E_{\rm c.m.}$ energies for the $^{16}$O+$^{238}$U reaction.

Figs. 1 and 6 show the increase of the quasifission cross section $\sigma^{\ell}_{qfiss}$ by increasing the collision energy $E_{\rm c.m.}$ but the fusion cross section $\sigma^{\ell}_{fus}$ also increases by $E_{\rm c.m.}$ more fastly than $\sigma^{\ell}_{qfiss}$ before saturation of $P_{CN}$. Favorable conditions for the formation of the evaporation residues in collisions with the large orientation angles $\alpha_T$ can be seen from the study of the fusion factor $P_{CN}$ which depends on $\alpha_T$. The fusion probability $P_{CN}$ is calculated by using the formula (11) of Ref.[18]

Fig. 7 shows the fusion probability $P_{CN}$ as a function of the collision energy $E_{\rm c.m.}$, for different values of the target orientation angle $\alpha_T$. Also the results of $P_{CN}$ confirm the conclusion that at $E_{\rm c.m.}$ <137 MeV only collisions with small $\alpha_T$ values (about $\alpha_T \leq 45^{\circ}$) can give an appreciable (small values) fusion probability $P_{CN}$. In such cases we obtain a reduction

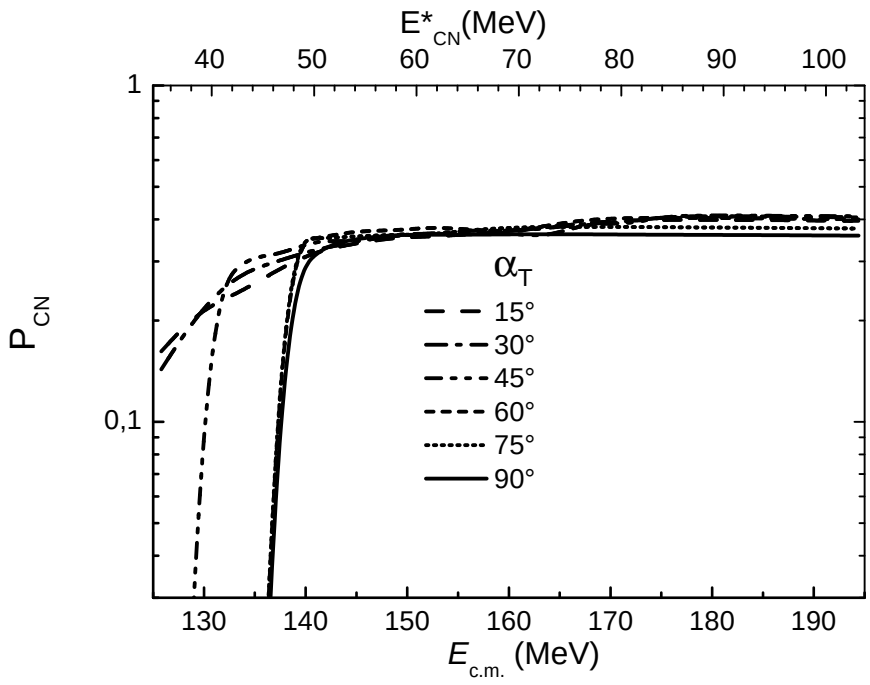


Fig. 7. Fusion probability $P_{CN}$ versus the collision energy $E_{\rm c.m.}$ for different values of the $\alpha_T$ angle. of the CN formation. By increasing the $E_{\rm c.m.}$ also the fusion probability increases and the contributions of collisions with large angles up to $\alpha_T = 90^\circ$ appear. At about $E_{\rm c.m.} > 150$ MeV the fusion probability $P_{CN}$ ranges around 0.35-0.41 with some saturation.

It is difficult to study quantitatively the dependence of the quasifission cross section as a function of $E_{c.m.}$ by the experimental data only because it is difficult to separate unambiguously quasifission fragments from the deep-inelastic collision, fusion-fission and fast-fission fragments.

The contribution of the quasifission process in the observed anisotropy of the fragment angular distribution was explored in Ref.[18] in the framework of the model based on the dinuclear system-concept: competition between complete fusion and quasifission is related to both values of the intrinsic fusion $B^*_{fus}$ and quasifission $B_{qf}$ barriers (see for example formula (11) in Ref.[18]).

According to our calculations increase of the yield of the quasifission fragments is explained by decreasing of the quasifission barrier $B_{qf}$. The small value of $B_{qf}$ means less stability of the dinuclear system during its evolution. There are two reasons leading to the decrease of the quasifission barrier: $B_{qf}$ decreases by increasing $\alpha_T$ (see Fig. 8(b)) and angular momentum $\ell$. Large values of both $\alpha_T$ and $\ell$ are populated by increasing $E_{\rm c.m.}$. In Fig. 8 we present the calculated values of the $B^*_{fus}$ and $B_{qf}$ barriers for the $^{48}$Ca+$^{154}$Sm reaction as a function of the orientation angle $\alpha_T$.

In the DNS model, $B^*_{fus}$ is determined as a difference of the values of the driving potential which corresponds to the initial mass asymmetry (solid squares in Fig. 9) and its maximum

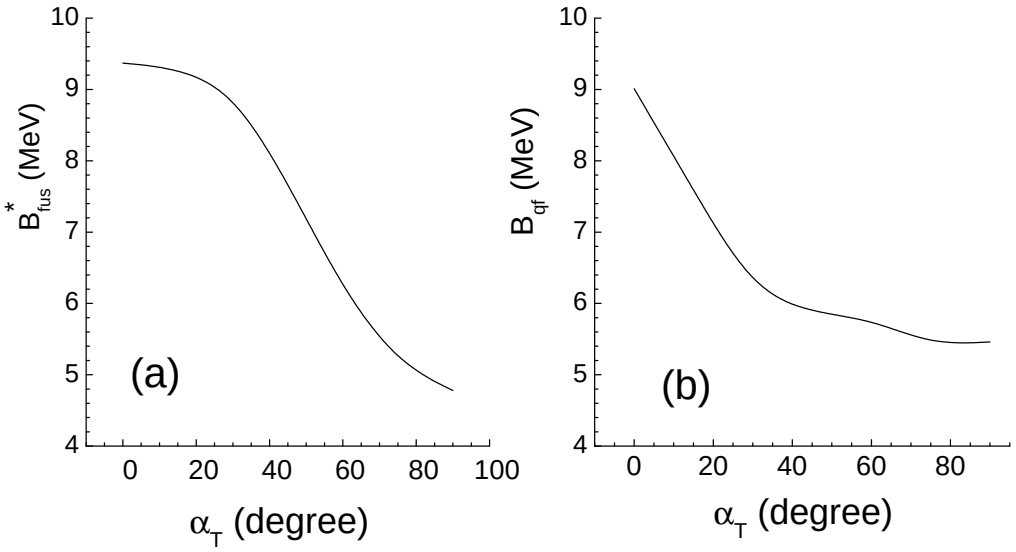


Fig. 8. Intrinsic fusion barrier $B^*_{fus}$ (a) and quasifission barrier $B_{qf}$ (b) for the initial charge asymmetry of the $^{48}$Ca+$^{154}$Sm reaction leading to the $^{202}$Pb compound nucleus versus the orientation angle $\alpha_T$ of the target–nucleus.

value in the way to the complete fusion along the mass asymmetry axis $Z \to 0$ (solid circles in Fig. 9). In the case of collisions of deformed nuclei, the values of $B^*_{fus}$ are larger for small orientation angles in comparison with the ones for large orientation angles of the symmetry axes of nuclei relative to the beam direction. In Fig. 9, the driven potential is presented in dependence on the values $\alpha_T$ for the$^{48}$Ca+$^{154}$Sm reaction. One can see that by the increase of the orientation angle $\alpha_T$ of the target leads to the decrease of the intrinsic fusion barrier $B^*_{fus}$ considered relative to the initial charge number $Z = 20$. As a result the fusion probability $P_{CN}$ that appears in formula (3) is sensitive to both values of the $B^*_{fus}$ and $B_{qf}$ barriers. But, as we have already stressed, the capture can occur at the large values of $\alpha_T$ only if we increase the beam energy allowing the system to overcome the Coulomb barrier.

Such values and trends of the barriers are consistent with the results that at lower $E_{\rm c.m.}$ energies only the small angles $\alpha_T$ can contribute to the $\sigma_{cap}$, $\sigma_{fus}$ and $\sigma_{ER}$ cross sections, by the relevant role of quasifission. At higher $E_{\rm c.m.}$ energies also large $\alpha_T$ configurations contribute to the above-mentioned cross sections.

Fig. 10 shows the excitation function of the evaporation residue formation, at various target orientation angles. At the smallest energy $E_{\rm c.m.}$=125.8 MeV (corresponding to $E^*_{CN}$=35.1 MeV of the compound nucleus) the main contributions to the evaporation residue cross section are given only by collisions with angular orientations of the target $\alpha_T < 30^\circ$. This is explained by the low values of the Coulomb barrier for such orientation angles $\alpha_T$ and by the appreciable probability (see Fig. 7) of complete fusion in competition with quasifission. In any case, at energies $E_{\rm c.m.} < 137$ MeV only collisions with the orientation angles about $\alpha_T \leq 45^\circ$ can contribute to the ER formation. At $E_{\rm c.m.} > 148$ MeV, collisions with all orientation angles contribute to the ER formation and the $\sigma_{ER}$ cross section ranges between 10–100 mb.

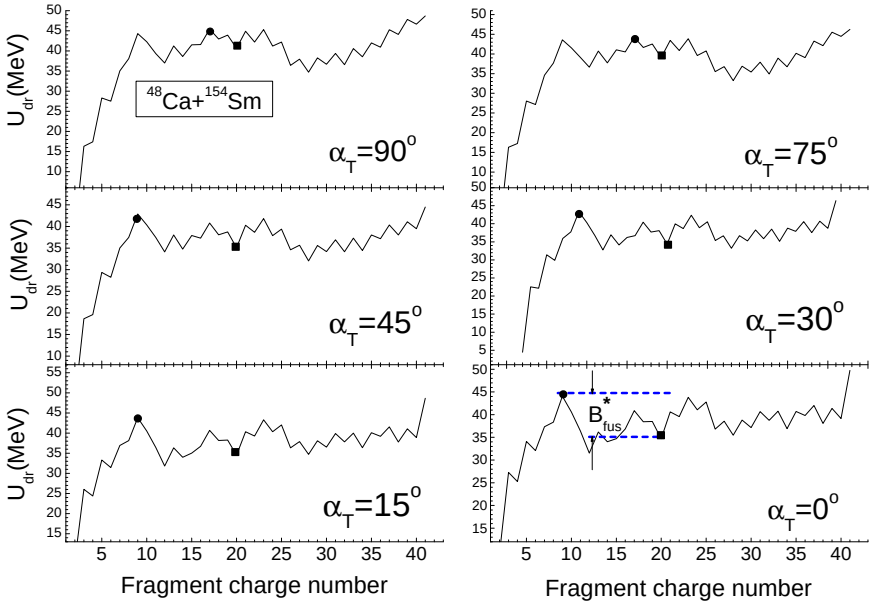


Fig. 9. The dependence of the driving potential $U_{dr}$ calculated for the dinuclear system formed in the $^{48}$Ca+$^{154}$Sm reaction for different values of the orientation angle $\alpha_T$. The difference between the values of $U_{dr}$ corresponding to the solid square at the initial charge asymmetry and solid circle on the maximum value of the driving potential is equal to $B^*_{fus}$.

The total ER yield reaches the maximum value (see also Fig. 1) with a saturation in the 148–158 MeV energy range. Then, at higher $E_{\rm c.m.}$ energies the formation of the evaporation residues decreases and at $E_{\rm c.m.}$ >180 MeV $\sigma_{ER}$ ranges around 0.1–10 mb. In spite of the approximately constant trend of the fusion probability $P_{CN}$ and fusion cross section $\sigma_{fus}$ at $E_{\rm c.m.} > 160$ MeV, the decrease of $\sigma_{ER}$ is explained by the increase of the excitation energy of the compound nucleus and its angular momentum which lead to a decrease of the fission barrier $B_f$ of the compound nucleus. The angular momentum distribution of the heated and rotated compound nucleus (and other intermediate nuclei along the de-excitation cascade of CN) plays a decisive role in calculation of its survive probability against fission, and then to the formation of the evaporation residues.[10] Another phenomenon leading to the decrease of $\sigma_{ER}$ at higher collision energies $E_{\rm c.m.}$ is the fast-fission process which is the splitting of the mononucleus into two fragments due to the absence of the fission barrier at very high values of the angular momentum $\ell > \ell_f$.

At least, we also discuss the result when we include in calculations the tunneling effect for the collisions at subbarrier fusion energy. This effect leads to the shift of the capture excitation function on 1.5–2.0 MeV to lower energies. In mass asymmetric reactions (for example $^{16}$O+$^{238}$U) the fusion cross section is nearly equal to the capture cross section and the enhancement of the subbarrier fusion can be seen in the cross section of the evaporation residues. In reactions with massive nuclei (with a higher mass symmetric parameter, as for example the

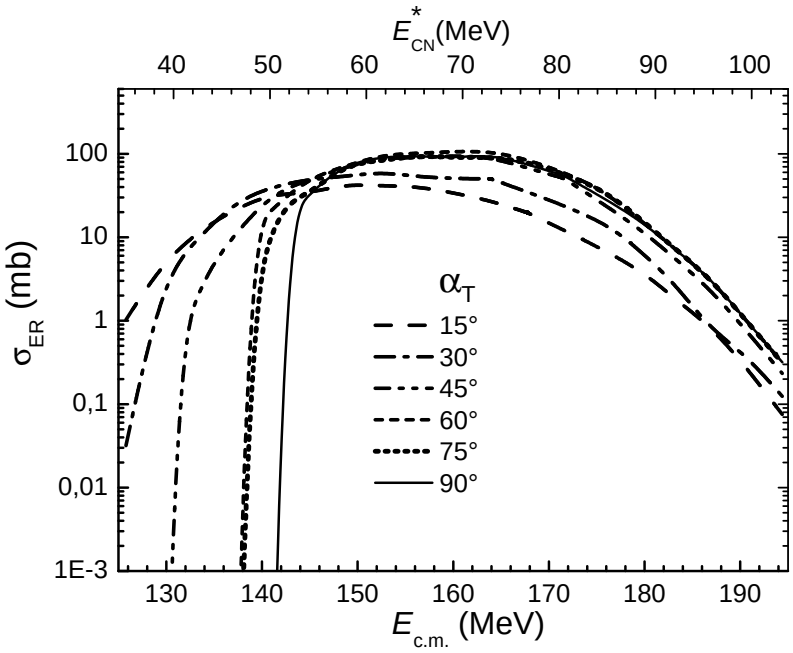


Fig. 10. Evaporation residue cross sections versus the $E_{\rm c.m.}$ energy for various orientation angles $\alpha_T$ of the $^{154}$Sm target.

$^{48}$Ca+$^{154}$Sm reaction), taking into account tunneling through the interaction barrier leads to an enhancement of the capture probability but this effect on the fusion excitation function for this reaction is very small. This is due to the intrinsic fusion barrier $B^*_{fus}$ which decreases the fusion probability at a given capture cross section. $B^*_{fus}$ is about 10 MeV for collisions with small orientation angles $\alpha_T$ and it decreases up to 5 MeV for large orientation angles (see Fig. 9). Due to the smallness of this effect on the results under discussion we do not present the results of such estimations.

## 4. Conclusions

In this paper the role of the orientation angle $\alpha_T$ of the symmetry axis of the deformed $^{154}$Sm nucleus on the complete fusion and evaporation residue cross sections is studied for the $^{48}$Ca+$^{154}$Sm reaction at energies near and above the Coulomb barrier. The dependence of the quasifission-fusion competition during the evolution of the dinuclear system and the sensitivity of the fission-evaporation competition during the de-excitation cascade of the compound nucleus on the values of the orientation angle $\alpha_T$ are demonstrated. The analysis of the dependence of the fusion and evaporation residue cross sections on the $\alpha_T$ angle shows that the observed yield of evaporation residues in the $^{48}$Ca+$^{154}$Sm reaction at low energies ($E_{\rm c.m.}$ <137 MeV) is formed at collisions with orientations $\alpha_T < 45^\circ$ because the collision energy is enough to overcome the corresponding Coulomb barrier. Only in this cases it is possible formation of the dinuclear system which evolves to the compound nucleus or breaks up into two fragments after multinucleon exchange without formation of the compound nucleus.

At high energies (about in the $E_{\rm c.m.}$ =148–180 MeV energy range) all orientation angles of the target-nucleus can contribute to $\sigma_{ER}$ and its values are included in the 10–100 mb interval. In spite of high collision energies (about $E_{c.m.}$ >158 MeV) the complete fusion still increases, the evaporation residue cross section $\sigma_{ER}$ goes down and its values range in the 0.1–1 mb interval due to the strong decrease of the survival probability against fission of the heated compound nucleus along de-excitation cascade. This is connected by the decrease of the fission barrier for a compound nucleus by increasing its excitation energy[10,11] and angular momentum.[15]

Another phenomenon leading to the decrease of $\sigma_{ER}$ at high energies is the fast-fission process which is the splitting of the mononucleus into two fragments due to absence of the fission barrier at very high the angular momentum $\ell > \ell_f$ where $\ell_f$ is the value of angular momentum at which barrier disappears.

From our study on the $^{48}$Ca+$^{154}$Sm reaction leading to the $^{202}$Pb compound nucleus we can affirm that in the explored energy range of collisions the quasifission is the dominant process in competition with the complete fusion for any orientation angle $\alpha_T$ of the symmetry axis of the deformed target–nucleus.

**Acknowledgment**

Authors thank Prof. R.V. Jolos, Drs. G.G. Adamian and N.V. Antonenko for fruitful discussions of this paper. G. Giardina and A.K. Nasirov are grateful to the Fondazione Bonino-Pulejo (FBP) of Messina for the important support received in the international collaboration between the Messina group and the Joint Institute for Nuclear Research of Dubna (Russia). One of authors A. Nasirov thanks INFN, Sezione di Catania, and Dipartimento di Fisica dell'Università di Messina for warm hospitality. This work was performed partially under the financial support of the RFBR and INTAS.

## References


1) S. Hofmann and G. Munzenberg: Rev. Mod. Phys. **72**, 733 (2000).
2) K. Morita, K. Morimoto, D. Kaji, T. Akiyama, S. Goto, H. Haba, E. Ideguchi, K. Katori, H. Koura, H. Kudo, T. Ohnishi, A. Ozawa, T. Suda, K. Sueki, F. Tokanai, T. Yamaguchi, A. Yoneda, and A. Yoshida: Jour. of the Physical Society of Japan, **76** (2007) 043201.
3) K. Morita, K. Morimoto, D. Kaji, T. Akiyama, S. Goto, H. Haba, E. Ideguchi, R. Kanungo, K. Katori, H. Koura, H. Kudo, T. Ohnishi, A. Ozawa, T. Suda, K. Sueki, H.S. Xu, T. Yamaguchi, A. Yoneda, A. Yoshida, and Y.L. Zhao: Jour. of the Physical Society of Japan, **73** (2004) 2593.
4) Yu. Ts. Oganessian, V. K. Utyonkov, Yu. V. Lobanov, F. Sh. Abdullin, A. N. Polyakov, I. V. Shirokovsky, Yu. S. Tsyganov, G. G. Gulbekian, S. L. Bogomolov, B. N. Gikal, A. N. Mezentsev, S. Iliev, V. G. Subbotin, A. M. Sukhov, A. A. Voinov, G. V. Buklanov, K. Subotic, V. I. Zagrebaev, M. G. Itkis,J. B. Patin, K. J. Moody, J. F. Wild, M. A. Stoyer, N. J. Stoyer, D. A. Shaughnessy, J. M. Kenneally, P. A. Wilk, R. W. Lougheed, R. I. Il'kaev and S. P. Vesnovskii: Phys. Rev. C**70** (2004) 064609.
5) K. Nishio, S. Hofmann, F.P. Hessberger, D. Ackermann, S. Antalic, V. F. Comas, Z. Gan, S. Heinz, J.A. Heredia, H. Ikezoe, J. Khuyagbaatar, B. Kindler, I. Kojouharov, P. Kuusiniemi, B. Lommel, R. Mann, M. Mazzocco, S. Mitsuoka, Y. Nagame, T. Ohtsuki, A.G. Popeko, S. Saro, H.J. Schott, B. Sulignano, A. Svirikhin, K. Tsukada, K. Tsuruta, A.V. Yeremin: Eur. Phys. J. A **29** (2006) 281.
6) A.K. Nasirov, A. Fukushima, Y. Toyoshima, Y. Aritomo, A.I Muminov, S. Kalandarov: Nucl. Phys. A **759** (2005) 342.
7) G. G. Adamian, N. V. Antonenko, W. Scheid, and V. V. Volkov: Nucl. Phys. A **633** (1998) 409c.
8) G. Giardina, S. Hofmann, A. I. Muminov, A. K. Nasirov: Eur. Phys. J. A **8** (2000) 205.
9) G. Giardina, F. Hanappe, A. I. Muminov, A. K. Nasirov, and L. Stuttgé: Nucl. Phys. A **671** (2000) 165.
10) G. Fazio, G. Giardina, A. Lamberto, R. Ruggeri, C. Saccá, R. Palamara, A. I. Muminov, A.K. Nasirov, U. T. Yakhshiev, F. Hanappe, T. Materna, L. Stuttgè: Eur. Phys. J. A **19** (2004) 89.
11) G. Fazio, G. Giardina, A. Lamberto, R. Ruggeri, C. Saccá, R. Palamara, A. I. Muminov, A.K. Nasirov, U. T. Yakhshiev, F. Hanappe, T. Materna, L. Stuttgè: J. Phys. Soc. Jpn. **72** (2003) 2509.
12) G. Fazio, G. Giardina, A. Lamberto, A. I. Muminov, A. K. Nasirov, F. Hanappe, and L. Stuttgé: Eur. Phys. J. A **22** (2004) 75.
13) A. K. Nasirov, G. Giardina, A. I. Muminov, W. Scheid, and U. T. Yakhshiev, in Proc. of the Symposium on Nuclear Cluster , Rauischolzhausen, Germany. Eds. Jolos, R.V.,and Scheid, W. 2003, (EP Systema, Debrecen), (2002) 415; A. K. Nasirov, G. Giardina, A. I. Muminov, W. Scheid, and U.T. Yakhshiev: Acta Phys. Hung. A **19** (2004) 109.
14) G. Fazio, G. Giardina, G. Mandaglio, F. Hanappe, A. I. Muminov, A. K. Nasirov, W. Scheid, and L. Stuttgé: Mod. Phys. Lett. A **20** (2005) 391.
15) A. J. Sierk: Phys. Rev. C **33** (1986) 2039.
16) G. Fazio, G. Giardina, G. Mandaglio, R. Ruggeri, A. I. Muminov, A. K. Nasirov, Yu. Ts. Oganessian, A. G. Popeko, R. N. Sagaidak, A. V. Yeremin, S. Hofmann, F. Hanappe, C. Stodel: Phys. Rev. C **72** (2005) 064614.
17) G. G. Adamian, R. V. Jolos, A. K. Nasirov, and A. I. Muminov: Phys. Rev. C **56** (1997) 373.
18) A. K. Nasirov, A. I. Muminov, R. K. Utamuratov, G. Fazio, G. Giardina, F. Hanappe, G. Mandaglio,

M. Manganaro, W. Scheid: Eur. Phys. J. A **34** (2007) 325.

19) H. Esbensen: Nucl. Phys. A **352** (1981) 147.
20) S. Raman, C.H. Malarkey, W.T. Milner, C.W. Nestor, Jr., and P.H. Stelson: Atomic Data and Nuclear Data Tables **36** (1987) 1.
21) R. H. Spear: Atomic Data and Nuclear Data Tables **42**, No. 1 (1989) 55.
22) A. D'Arrigo, G.Giardina, M. Herman, A. V. Ignatyuk, and A. Taccone: J. Phys. G **20** (1994) 365.
23) A. D'Arrigo, G. Giardina, M. Herman, and A. Taccone: Phys. Rev. C **46** (1992) 1437.
24) A. M. Stefanini, M. Trotta, B.R. Behera, L. Corradi, E. Fioretto, A. Gadea, A. Latina, S. Szilner, Y.W. Wu, S. Beghini, G. Montagnoli, F. Scarlassara, A.Y. Chizhov, I.M. Itkis, N.A. Kondratiev, I.V. Pokrovskiy, R.N. Sagaidak, G.N. Kniajeva, E.M. Kozulin, V.M. Voskressensky, S. Courtin, F. Haas, N. Rowley: Eur. Phys. J. A **23** (2005) 473.
25) M. Warda, B. Nerlo-Pomorska, K. Pomorski: Nucl. Phys. A **635** (1998) 484.
26) A.B. Migdal, Theory of the Finite Fermi-Systems and Properties of Atomic Nuclei (Moscow, Nauka, 1983).
27) D.J. Hinde,M. Dasgupta, J.R. Leigh, J.C.Mein, C.R.Morton, J.O. Newton, H. Timmers: Phys. Rev. C **53** (1996) 1290.